IEEE Access
Multidisciplinary | Rapid Review | Open Access Journal

Received July 18, 2020, accepted July 24, 2020, date of publication August 6, 2020, date of current version August 21, 2020.

Digital Object Identifier 10.1109/ACCESS.2020.3014701

Region-of-Interest Based Transfer Learning Assisted Framework for Skin Cancer Detection

REHAN ASHRAF[1], SITARA AFZAL[2], ATTIQ UR REHMAN[3], SARAH GUL[4], JUNAID BABER[5], MAHEEN BAKHTYAR[5], IRFAN MEHMOOD[6], (Member, IEEE), OH-YOUNG SONG[7], AND MUAZZAM MAQSOOD[2]

[1]Department of Computer Science, National Textile University, Faisalabad 37610, Pakistan
[2]Department of Computer Science, COMSATS University Islamabad, Attock Campus, Attock 43600, Pakistan
[3]Department of Computer Science, CECOS University, Peshawar 25000, Pakistan
[4]Department of Biological Sciences, FBAS, International Islamic University Islamabad, Islamabad 44000, Pakistan
[5]Department of Computer Science and Information Technology, University of Balochistan, Quetta 87300, Pakistan
[6]Department of Media Design and Technology, Faculty of Engineering and Informatics, University of Bradford, Bradford BD7 1AZ, U.K.
[7]Department of Software, Sejong University, Seoul 05006, South Korea

Corresponding authors: Muazzam Maqsood (muazzam.maqsood@cuiatk.edu.pk) and Oh-Young Song (oysong@sejong.edu)

This work was supported in part by the Ministry of Science and ICT (MSIT), South Korea, through the Information Technology Research Center (ITRC) Support Program supervised by the Institute for Information & Communications Technology Planning & Evaluation (IITP) under Grant IITP-2020-2016-0-00312, and in part by the Faculty Research Fund of Sejong University in 2019.

ABSTRACT Melanoma is considered the most serious type of skin cancer. All over the world, the mortality rate is much high for melanoma in contrast with other cancer. There are various computer-aided solutions proposed to correctly identify melanoma cancer. However, the difficult visual appearance of the nevus makes it very difficult to design a reliable Computer-Aided Diagnosis (CAD) system for accurate melanoma detection. Existing systems either uses traditional machine learning models and focus on handpicked suitable features or uses deep learning-based methods that use complete images for feature learning. The automatic and most discriminative feature extraction for skin cancer remains an important research problem that can further be used to better deep learning training. Furthermore, the availability of the limited available images also creates a problem for deep learning models. From this line of research, we propose an intelligent Region of Interest (ROI) based system to identify and discriminate melanoma with nevus cancer by using the transfer learning approach. An improved k-mean algorithm is used to extract ROIs from the images. These ROI based approach helps to identify discriminative features as the images containing only melanoma cells are used to train system. We further use a Convolutional Neural Network (CNN) based transfer learning model with data augmentation for ROI images of DermIS and DermQuest datasets. The proposed system gives 97.9% and 97.4% accuracy for DermIS and DermQuest respectively. The proposed ROI based transfer learning approach outperforms existing methods that use complete images for classification.

INDEX TERMS Melanoma detection, skin cancer detection, ROI, CNN, transfer learning.

I. INTRODUCTION

Skin cancer is considered as one of the common and dangerous types among other cancers [1]. Recent surveys show that the rate of patients infected by skin cancer is increasing every year as compared to other cancer types [2]. There are many types of skin cancer and melanoma is one of the most common types. It influences melanocytes which are the skin surface cells. It contains different kinds of cells that cause the skin to get darker [3]. Sometimes it is found in different dark shades. It is also found in the skin in different colors including rosy pink, royal purple, azure or it can be colorless as well [4]. Its ability to spread rapidly makes it more dangerous and fatal. Melanoma can be found anywhere on the human body even though it mainly grows on the backside of a person's lower limb [5]. In individuals, risk factors of skin cancer disease can be reduced by detecting it timely or before time in an early stage. Generally, a significant reduction in the mortality rate can be achieved by detecting skin cancer in its early stages. Therefore, the identification and classification of this disease in its initial stages are significant [4], [5].

The ABCD rule is usually used by the physicians to identify nevus and melanoma [5]. A total dermoscopic score is used for ABCD rule, where A indicates the asymmetry, the border irregularities are represented by B, C representing color variations, and D representing the diameter. Individual weight is allocated for every particular feature based on their importance. The classification of the lesion into cancerous or

The associate editor coordinating the review of this manuscript and approving it for publication was Pengcheng Liu.

non-cancerous is based on total dermoscopic score. Another method called A7-point Checklist is utilized for skin cancer identification.

This A7-point list focuses on indications of the atypical color network, grey-blue regions, atypical vascular shape, bands, blemishes, uneven dots and blobs, and regression models. A medical professional is consulted when these symptoms are identified [6]. Afterward, the size of the checklist cut down to a less number of features, symmetry, and blue-white structures [7]. A complex nature and structure of melanoma makes it difficult to identify handcrafted features according to nature, color, texture, and the shape of the cancer cells. Another issue is skin cancer image repositories are growing dramatically. Therefore, the practicality of computer-aided solutions is based on types of images, skin cancer cell's color, and how well the data can be retrieved.

Generally, researchers emphasize on automatic classification and identification of cancer using computer-aided diagnostic systems. For this purpose, skin cancer medicinal images in the form of textual [8]–[10] geometric [4] [11]–[13], color, and combination of features [14]–[16] have been utilized. Though, identifying the initial stages of melanoma using discriminative features is still a challenging task [17]. To use handcrafted features for melanoma detection, experts need to have a good understanding of skin cancer type, color of skin, shape, and texture. To overcome this issue, the trend is shifting towards fully automated deep learning-based CAD solutions for skin cancer. However, there is still a need to work on these deep learning-based solutions because of limited labeled data availability. The class imbalance issue is another problem for skin cancer detection. To design a fully automated accurate CAD solution which automatically detect discriminative features without human intervention remains a challenging task.

From this line of research, we propose a fully automated deep learning-based CAD solution that uses preprocessed images that only contains skin cancer regions instead of full images. As, to train a network on CNN, a huge number of samples are required for all classes [5] and the unavailability of this data creates problems [14]. The DermIS and DERQUEST both datasets are publicly available but contains less amount of data required for deep learning. In classification, these lesser samples lead to unexpected inaccuracies and can even cause critical issues in medical imaging because of imbalanced classes. To overcome these issues, the pre-trained CNN model AlexNet is utilized for the automatic classification of skin cancer. The data got from both datasets i.e. DermIS and DERQUEST were augmented for equalizing the samples of both classes. We extract the Region of Interest (ROIs) that only contain the required region. This helps the model to train itself on specific regions which ultimately results in better feature learning. The proposed work uses ROIs extracted from improved k-mean algorithm [18] and then apply augmentation to increase the samples and to handle class imbalance problem. These images are then classified using a transfer learning technique which gives excellent results. The paper has the following contributions:

- We propose a fully automated transfer learning-based improved CAD solution to detect melanoma accurately
- We design a Region of Interest-based approach that extract discriminative features without human expert intervention
- We design an augmentation-based CAD for melanoma to handle class imbalance problem

The rest of the paper is structured as follows; a thorough literature review of the current state-of-the-art approach in section II. The proposed methodology is explained in detail in section III. The experimental setup and results are explained in section IV followed by the conclusion of the paper.

II. LITERATURE REVIEW

For the classification of melanoma disease, various approaches including the ABCD-E scheme [11], [13], [19], a checklist of 7-points [20], [21], and a 3-point checklist [7] were used in different systems. In [12], researchers proposed that the computational cost of extracted features from the ABCD scheme is less expensive as compared with the checklist of 7-point. It is also observed that ABCD achieved a high consistency rate with clinical diagnosis. Therefore, mostly CAD systems for the diagnosis of melanoma utilized the ABCD scheme for feature extraction. However, this approach is more prone to nevias melanomas during classification [22]. Kasmi and Mokrani [4] combined the color asymmetry and dermoscopic structure with features extracted from ABCD and attained 91.25% sensitivity. In[23], a transfer learning approach was used for medical images to extract the features from the MRI and then they utilized a support vector machine for classification. This technique was useful to reduce the false positives. In [24], a deep learning-based framework was used to automatically detect dermoscopic patterns and achieved 88% accuracy. Moussa *et al.* [25] also utilized this scheme without considering color features as it requires more computational resources and achieved 89% accuracy using KNN.

This is noticeable that ABCD rubrics are subjective which results in a high inter as well as intra-observer bias [26]. Therefore, a high-quality initiative feature technique was utilized to represent the asymmetry characteristic of ABCD rubrics skin cancer images [27]. The proposed system achieved 86% performance accuracy. Amelard et. al. [9] extended his findings by adding new high-quality initiative features for distinct color channels and achieved 94% accuracy. The color features can be extracted using statistical values of color channels. Few other colors extracted approaches include color's irregularity, centroid distance, and LUV histogram distance [25], [28], [29]. In [30], another group of researchers classifies melanoma skin cancer based on local and global features. They achieved 93% accuracy by combining textual features with color features.

Some other researchers utilized the same approach but in addition to textual and color features, they also utilized shape-based features. Ganster *et al.* [31] used the KNN classifier along with colored and shaped features from lesion skin. For training, 5300 images were taken and obtained 87% sensitivity and 92% specificity. Rubegni *et al.* [32] used textual and geometrical features as well and achieved the same sensitivity and specificity of 96%. Celebi *et al.* [28] used a feature vector of shape, texture, and color features with SVM and achieved 93% sensitivity and 92% specificity. Almansour and Jaffar [14] utilized the SVM classifier with color and textual features and attained 90% performance accuracy. The textual feature of the image represents the spatial distribution of pixel intensity levels. Textural features show intensity levels' underlying pattern and layout and serve as one of the most discriminative features for object or ROI detection. The textural features are generally used for skin cancer analysis as it calculates structural irregularity between nevus and melanoma cancer classification [33].

It has been observed that the computerized examination is getting popular. Epilu-computerized microscopy (ELM) based method was proposed to enhance the initial diagnosis of a melanoma classification scheme for the computerized analysis [31]. ROI was extracted by utilizing the segmentation algorithms and the merged featured approach was utilized based on the shape and radiometric features. K Nearest Neighbor was utilized and attained 87% and 92% sensitivity and specificity respectively. The automated analysis of data for the melanoma initial recognition scheme[34] achieved 80% for both specificity and sensitivity utilizing asymmetry and boundary descriptor with Support Vector Machine as a classifier.

Iyatomi *et al.* [35] utilized a similar technique and achieved 100% specificity and 95% sensitivity. In [36], researchers achieved 91% and 88.2% specificity and sensitivity respectively trained over 120 cancer images. In [36], the researcher utilized active contour and watershed methods for the segmentation. They extracted shape, color, and texture related features. This proposed architecture was trained on 50 DermIS datasets and attained 80% performance accuracy. A new CAD technique of early identification of melanoma was proposed for web and android phone applications. All the images were taken from high definition cameras rather than utilizing any repository [37]. The proposed system utilized digital cameras with context information like kind of skin, span, and all the affected parts of the body. The proposed architecture also tried to remove the Dermoscopic ADCD compatible features. This attribute was then classified in numerous phases including a pre-processing phase for selection of association-based attributes. This scheme attained 68% specificity and 94% sensitivity on 45 nevus and 107 melanoma skin cancer datasets.

The Authors in [38] extracted ROI utilizing K-Mean clustering and textural color extracted attribute on non-demographic skin cancer images. Moreover, a collection of pictorial features was identified by examining the physician. The feature extraction was utilized for the automatic classification of skin cancer. To attain the final classification, a majority vote was utilized. The recommended technique caused in advanced analytic of 81% and attained higher accuracy as compared with the latest findings. In [39], researchers have represented the melanoma lesion through a feature vector comprising textual, shape, color data, and local-global features. In [40], [41], another classification and diagnosis of melanoma skin cancer were proposed to enhance the classification of skin lesions. In [42], the researcher proposed an approach for feature selection which was constructed on the arrangement of differential evolution and Support Vector Machine. In [43]–[47] researchers extracted features using machine learning techniques for skin cancer detection.

In recent years, deep learning and CNN are utilized for diagnosis of skin cancer but computational cost remains a problem [2], [48], [49]. In the new findings, Dorj *et al.* [50] proposed a classification approach for different cancer types by utilizing CNN. They used pre-trained AlexNet to extract features from the image and ECOC SVM utilized as a classifier for the classification of cancer and achieved 90% accuracy. In [51], an improved computer-automated system was proposed along with pixels centered based segmentation approach. They extracted features by CNN but classified them using the SVM classifier and achieved 93% accuracy on the DermIS dataset. All the referred approaches give promising results, but they are validated on inadequate data. It has been observed that existing work is more focused on extracting and selecting discriminative features using human expert knowledge for this problem.

These handcrafted features selection requires a good knowledge of the domain and it is also time taking. These handpicked features require human intervention and therefore, these are not fully automated. The deep learning-based methods use full images for feature extraction and usually, the region of interest is not that large. Therefore, the original large images may have an impact on the overall feature learning of deep learning models. Furthermore, deep learning generally requires a huge amount of labeled data for better performance and to avoid overfitting. Considering all these aforementioned limitations of the existing work, we propose a fully automated solution for skin cancer detection. We extract the ROIs from the image which excludes the background from the image and then these segmented ROIs are further used for processing. In our proposed work, we have designed a system that can automatically extract discriminative features from ROIs. The proposed system also performs data augmentation to handle class imbalance issues. Furthermore, the transfer learning approach is used to learn low-level features to improve the learning as compared to a previous study where it was efficiently used to reduce the false positives in the CAD system [23].

III. PROPOSED METHODOLOGY

In this section, the detail of our proposed model is presented in the following subsections. The input data taken from

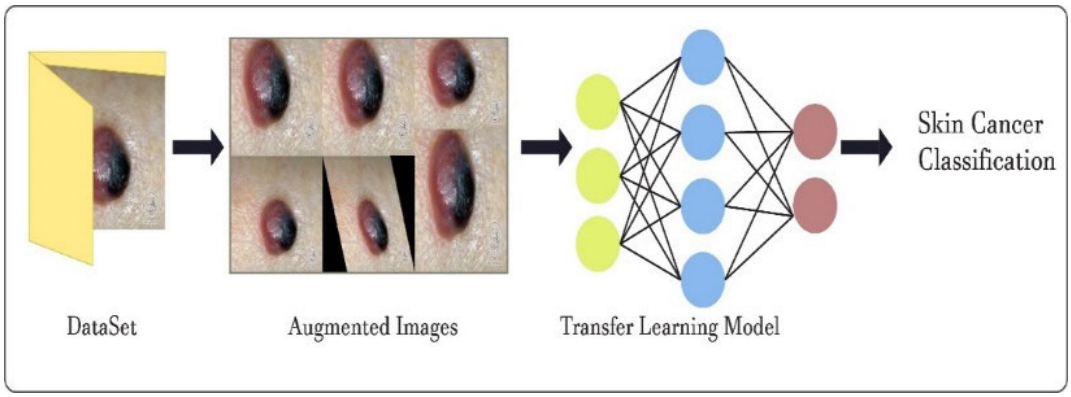

FIGURE 1. Skin cancer original data classification.

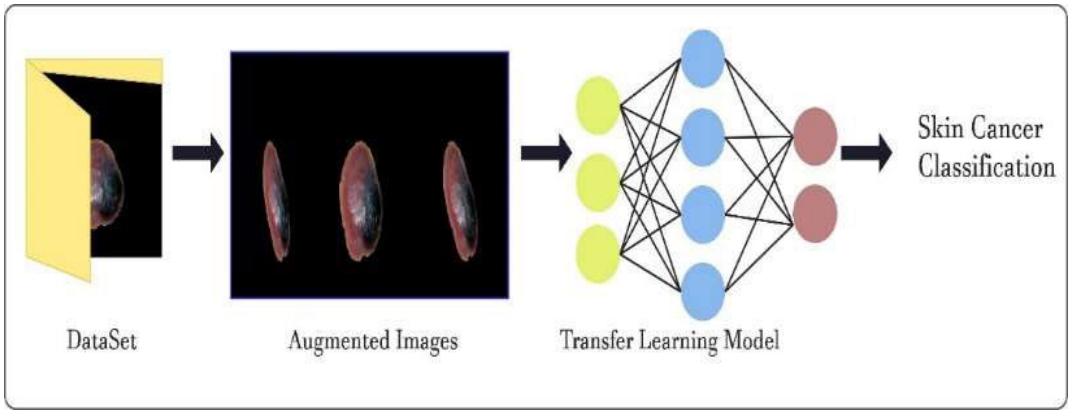

FIGURE 2. Skin cancer region of interests classification.

a publicly available repository undergo preprocessing for quality enhancement. To extract discriminative features and efficient classification, ROI was extracted from the samples. Figure 1 shows the proposed methodology without segmentation of ROI from the data (for comparison) and Figure 2 demonstrates the proposed methodology of the Region of Interests data samples.

A. PRE-PROCESSING

Medicinal images are frequently susceptible to noise mostly because of low light, fur, and air bubbles [52]. In images, the presence of this noise results in artifacts. Because of these kinds of artifacts, segmentation may get affected and causes inaccurate detection results. Therefore, noise removal is an important preprocessing step before the application of any segmentation or feature extraction approach. The Gaussian kernels are highly recommended for smoothing image as it eliminates noise that can be there at the time of acquisition. This kernel coefficient is modeled from the 2-dimensional function of Gaussian. The pre-processing step is illustrated in Figure 3. Equation 1 shows the Gaussian function: σ shows the smoothing factor.

$$G(a, b) = \frac{1}{\sqrt{2\pi\sigma^2}} e^{-(a^2 + b^2)} \Big/ 2 * \sigma^2 \qquad (1)$$

B. SKIN CANCER REGION OF INTEREST SEGMENTATION

We used an ROI based approach because the Region of Interest is vital to locate the lesion area accurately. ROI helps in training by improved discriminative feature learning in the skin cancer classification. The features extracted only from a lesion are more important as compared to the features extracted from the whole image (global features). We extracted ROI from the actual images by using the improved K-mean algorithm. K-Mean is extensively utilized in numerous applications of machine learning techniques, including Data Mining, Image Processing, and pattern recognition [16]. It splits the images to a non-overlapping cluster of pixels depends on intensity levels. The pixels of the images are grouped in an exclusive way such that if any pixel value or data point belongs to a specific cluster, it will not mix with other clusters. This procedure starts by choosing the center point from data points and we used an improved procedure for centroid selection [18] rather using random centroids. All the image pixels or data points are grouped depends on the distance that is a minimum distance from a center point. Once the iteration is completed, a new center point usually referred to as centroid is selected by taking the mean and set that mean as the center point for the next iteration. This iterative process repeats until there is no alteration in the

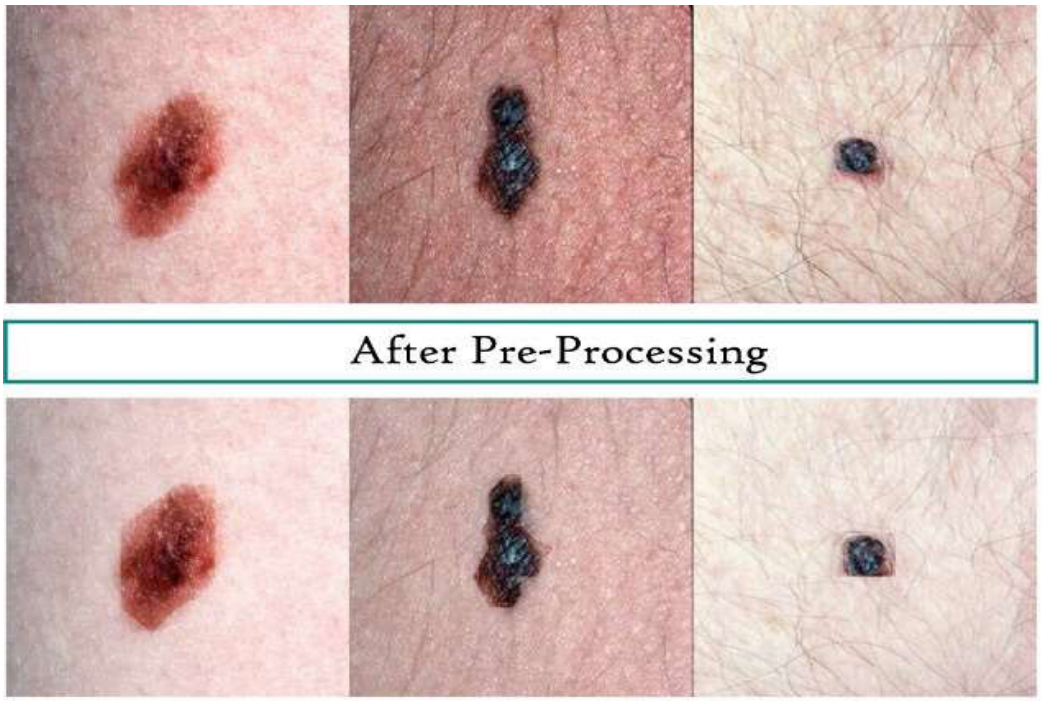

FIGURE 3. Before and after image pre-processing samples.

FIGURE 4. Segmented ROI images samples.

successive cluster centroid. Figure 3 shows the segmentation of the image, where a left image is an original image.

The proposed K-mean initializes its center point by the center point selection techniques as given in equation 2.

$$mu = (1 : K) * \frac{\mathrm{m}}{k+1} \tag{2}$$

In the equation 1, K represents the number of clusters, the maximum pixel value is shown by m and the value of k is vary from 1 to K. The approach of selecting the center point works by ensuring major changes amongst the starting center point values. It also makes it robust and effective by converging to the final position in a lesser number of iterations. The input images in our proposed methodology contain background images with an affected mark or lesion. We take the K = 2, the background skin is removed from the foreground affected mark and can be seen in Figure 4. The segmented images are not of equal sizes, to deal with this, we resized all the images after segmentation in the 227 × 227 dimension to training the neural network.

C. SKIN CANCER DATA AUGMENTATION

A great amount of data models leads to affect the distribution of many CNN [4]. The problem that might happen in the training of inadequate data is overfitting. Usually, the training data available for all classes are not equally distributed which leads to class imbalance problem. In this skin cancer study, looking at the inadequate data samples we

FIGURE 5. Sample of melanoma augmented images.

extend the image samples by applying common augmentation techniques including cropping the original images from the right, left and from the bottom side, flipping, mirroring, and rotation at the 270° and get 7 new unique samples from each image.

The data samples belong to class label melanoma and non-melanoma are increased using this augmentation technique. The reason to select this technique was to produce new unique images to prevent overfitting and class imbalance issues to enhance performance accuracy. So, we extend existing samples of segmented as well as original samples by applying distinct augmentation approaches on both the datasets i.e. DermQuest and DermIS. Figure 5 shows the sample augmented images that we generate by applying different augmentation approaches.

D. SKIN CANCER DIAGNOSIS USING TRANSFER LEARNING APPROACH

After the augmentation of data samples, we resized images as per AlexNet requirements. For training the new CNN model, current data has inadequate samples. So, to handle this issue, the transfer learning approach is used. This pre-trained model learns low-level features from AlexNet and then uses this training on a new actual dataset.

AlexNet is the commonly used model in classification and pattern recognition tasks. In the AlexNet model, there are a total of eight layers including 5 convolutional layers and three fully connected layers. The pre-trained AlexNet is applied when all the augmented data is equal to every input class. In the AlexNet framework, there are max-pooling layers between the first two convolutional layers. A pooling layer is a new layer added after convolutional layers to reduce the size of the feature map. During the training procedure, a small learning rate is used because a smaller learning rate gives smaller changes to update weight. The detailed steps of the methodology for skin cancer using transfer learning are shown in Figure 6. In the next subsections, the structure of the pre-trained AlexNet model is explained in detail.

1) FIRST INPUT LAYER

In this first input layer of CNN, all the resized augmented data are given as an input on this layer.

2) CONVOLUTIONAL LAYERS

Convolutional layers are the primary layers in whole CNN as all the task related to computational is accounted by these layers. It mainly performs convolutional tasks on the input and then sends that response to the next required layer of the model. The convolutional layers allow layer close to the input to learn low-level features and a deeper convolutional layer learns high features or class-specific features.

3) MAX-POOLING LAYERS

In between the convolutional layers, there are pooling layers that are responsible for the reduction of pixel representation as well as computational cost. To reduce the computational cost for the next layer, the pool layer work on each pixel of the image. It works just like filters to be applied to the feature map.

The size of the feature map is much greater than the pooling layer size. Almost the pooling layer has 2×2 size with a stride of 2 pixels, which means the pooling layer will always reduce the size of the feature map by a factor of 2. In our model, the max-pooling layer was added in between convolutional layers to calculate maximum value for each feature map.

4) FULLY CONNECTED LAYERS

From the input images, the size of the feature map was extracted and reduced because of convolutional and max-pooling layers. The final output is equal to the number of

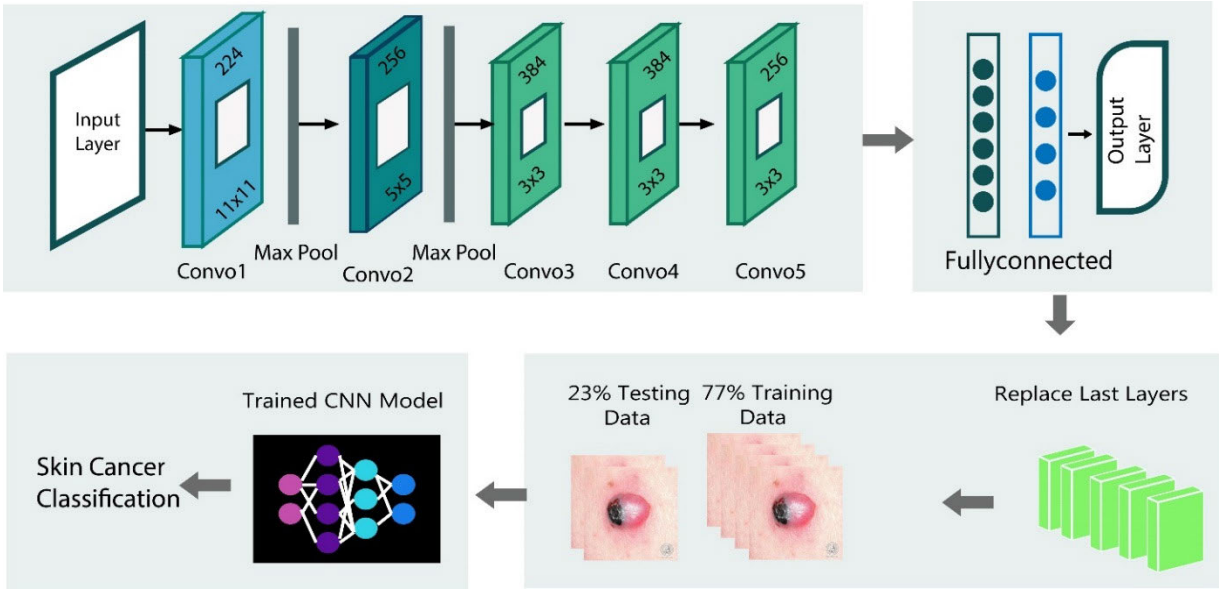

FIGURE 6. Complete transfer learning flow diagram.

classes produced by applying layers that are fully connected. In AlexNet structure, first convolutional layers do filtration on images with dimensions 227 × 227 ×3 along with 96 kernels of dimensions 11 × 11 in which 227 × 227 is width and height and 3 represent Depth, refer to red, green and blue respectively. The feature map taken from the convolutional layer is passed through the max-pooling layer to reduce features and forwards this new feature map to the next second convolutional layer having 256 kernels of size 5 × 5 ×48. Similarly, the results of the second convolutional layer are then reduced by the max pool layer having 384 kernels in the number connected with a third convolutional layer. The last three convolutional layers are interconnected without having any max-pooling layer.

There is a total of 384, 256 numbers of the kernel in fourth and fifth convolutional layers, respectively. After all the convolutional layers and max-pooling layers, high-level reasoning in the neural network is done by fully connected layers. In fully connected layers the number of neurons is 4096. The fully connected layers connect every neuron in one layer with every neuron in the next layer. Neurons in the fully connected layers have a connection with all activation in previous layers.

5) REPLACING LAST LAYERS

Normally the low-level features that are mainly edges, lines, and patterns, are on the initial layer of the network whereas the class-specific feature is on the last layer of the network. So, our concern is with the skin data training. For this reason, we replaced class-specific features with new layers which means we replaced the classification layer with the Soft-Max layer and fine-tuned all weights. The feature map from convolutional layers is moved and replaced with the layers having class-specific features. We used different parameters such as weight learn factor, Bias learn factor for making the fully connected layers. These training parameters control the learning rate of the network.

6) NETWORK TRAINING AND TESTING

In this network, there are five transferred layer and three new layers for adaptation. Initially, the data sample has an inadequate number of samples for the training network. We have overcome the issue by augmentation and transfer layers. We have utilized augmentation approaches for both the training and testing datasets. Only the new layer is trained for accurate classification of cancer.

We take 77% of the data for training and pass it into a network with some training options such as epochs, batch sizes, and learning rates. We train the network on a 1-10 epoch size. Measuring the performance of training methodology in a trained network, we then permit the remaining 23% data as testing data. We measure the trained network performance based on the accuracy metric.

IV. EXPERIMENTAL RESULTS AND DISCUSSION

A. DATASET

We have used two datasets i.e. DermIS [14] and DermQuest for skin cancer diagnosis. There is a total of 146 whereas in DermQuest the number of samples is 76. All the results from our findings are briefly discussed in the form of classification performance. We divided the images into two parts taken from datasets namely train and test. We split the images into a 77% and 23% ratio. Partitions of both the parts are guaranteed of having both melanoma and not melanoma case and are balanced with the augmentation approach. All the experiments are performed using MATLAB_2018b with a 6GB NVIDIA GPU card. Table 1 shows the detail of the data samples.

TABLE 1. Detailed dataset.

Images	DermIS Melanoma	DermIS Non-Melanoma	DermQuest Melanoma	DermQuest Non-Melanoma
Original Images	146	251	76	61
Augmented Images	1022	1757	532	427

B. PERFORMANCE EVALUATION

Accuracy has been widely used for performance evaluation in medical imaging [53]–[57]. It can be described as:

$$A_c/A_t^*100 \tag{3}$$

The accurately classified output is representing by Ac, whereas the total classified output is representing by At.

C. RESULTS FOR DermIS AND DermQuest USING AUGMENTATION

In this section, we have presented the results of classification with data augmentation technique on both the dataset i.e. DermIS and DermQuest.

1) RESULTS FOR DermIS

All the experimentations conducted using a color image from the required database, as per the AlexNet, the image size should be 227 × 227 ×3. Thus, it is guaranteed that the required size of images is according to the required dimensions. The convolutional network parameter utilizes a classification of the ImageNet database. In this transfer learning model, the feature extraction and then classification process is fully automated. We fine-tuned the model by changing different parameters. To achieve the optimal results, we investigated all training options. We checked the learning rate by varying values from le-1 up to le-10. In the same way, to reach optimum output we vary the bias and weight learn factor from le-4 to le-10 and 10-100 respectively. To find the optimum amount of epoch, binary class classification is performed by utilizing the transfer learning model on epoch 6, 7, and 8.

Figure 7 demonstrates the Training and Loss process of the DermIS Region of Interest Data on epoch 9 using augmentation techniques. We achieved 97.9% performance accuracy utilizing the ROI images on epoch 9 with the different augmentation approaches.

There is a 2% increase in performance that is achieved in contrast with the output from epoch 7 with epoch 9.

For skin cancer classification, we calculated the output achieved from the epoch 6, 7, and 8 with the approaches of augmentation on data and concluded that epoch 9 gives the most optimum classification results. The model of AlexNet learn the data in training and reached 94.44% performance accuracy on the very epoch1, 90.28% on epoch 2, 95.83% on epoch 3, 96.8% on epoch 4, 95.83% on epoch5 and 96.1% on epoch6 and 96.4% on epoch7 for binary class skin cancer

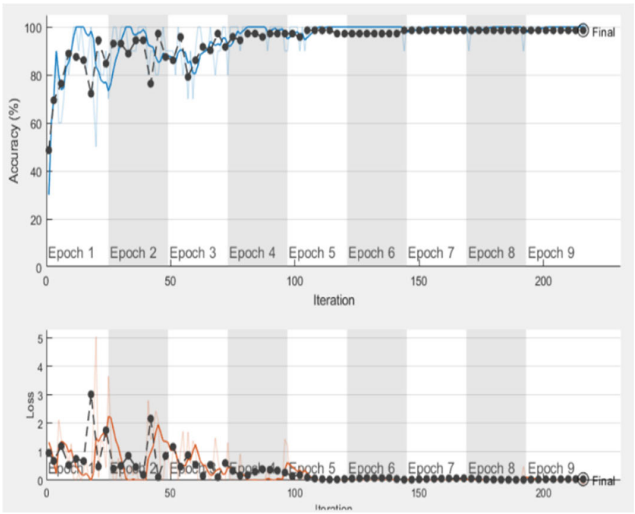

FIGURE 7. Training and loss process of DermIS ROI with augmentation on epoch 9.

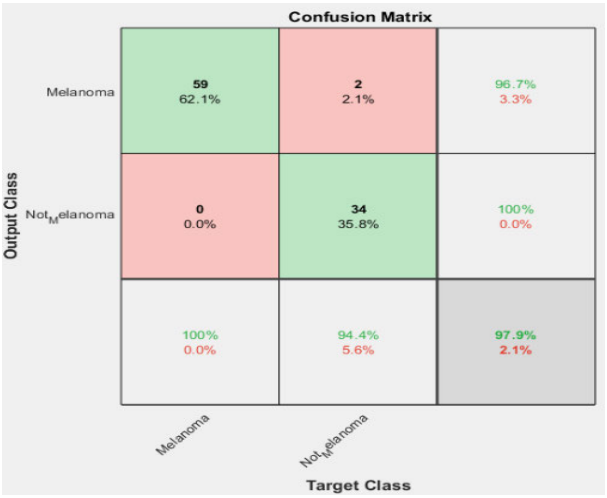

FIGURE 8. Confusion matrix of DermIS ROI with augmentation on epoch 9.

classification. Figure 8 shows the confusion matrix of ROI DermIS data with augmentation generated during the training at epoch 9.

We performed this transfer learning approach to the original DermIS data as well with approaches of data augmentation for a fair comparison. Figure 9 demonstrates the training

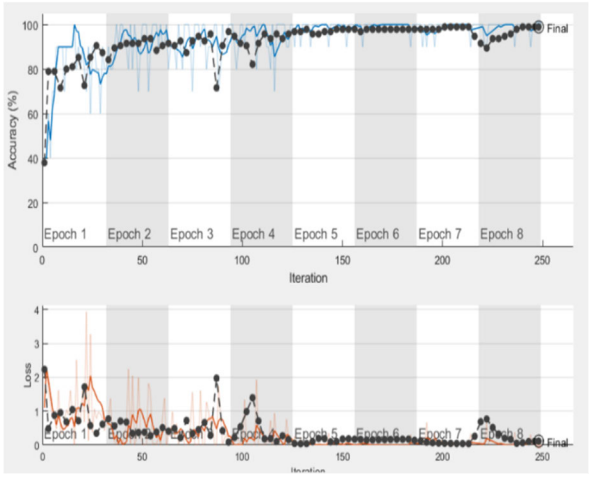

FIGURE 9. Training and loss process of original DermIS with augmentation on epoch 8.

and loss process of original DermIS images for epoch size 8. We achieved 97.2% performance accuracy using original DermIS images on epoch size 8. We calculated the outputs achieved from epochs 6, 7 and 8 with augmentation approaches and concluded that epoch 8 gives the optimum output.

The blue lines in the figure show the training process whereas black dotted lines represent the validation process. This AlexNet architecture acquires the training data and reached 82.11% accuracy on epoch 1, 89.47% on epoch 2, 90.84% on epoch 3, 92.63% on epoch 4, 91.58% on epoch 5 and 95.79% on epoch 6 and 89.47% on epoch 7 for binary class skin cancer classification. Figure 10 shows the confusion matrix of DermIS data with augmentation generated during the training at epoch 8.

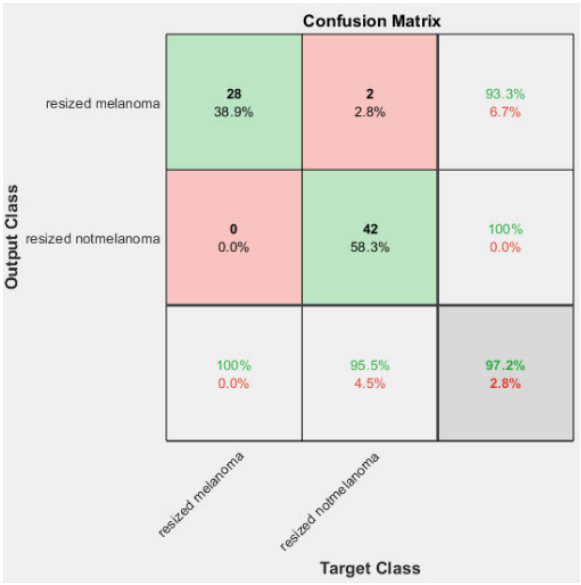

FIGURE 10. Confusion matrix of DermIS original images with augmentation at epoch 8.

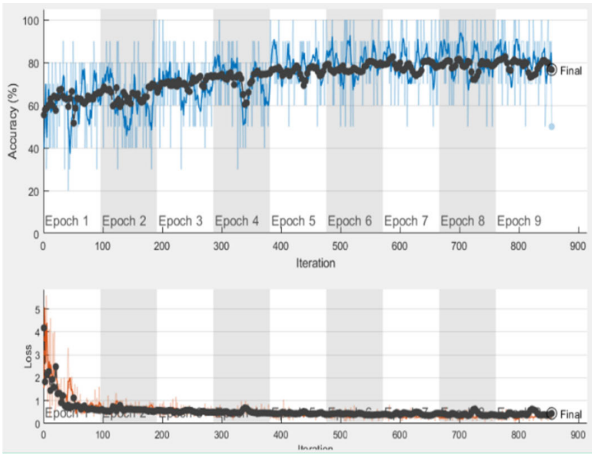

FIGURE 11. Training and loss process of original DermQuest with augmentation on epoch 9.

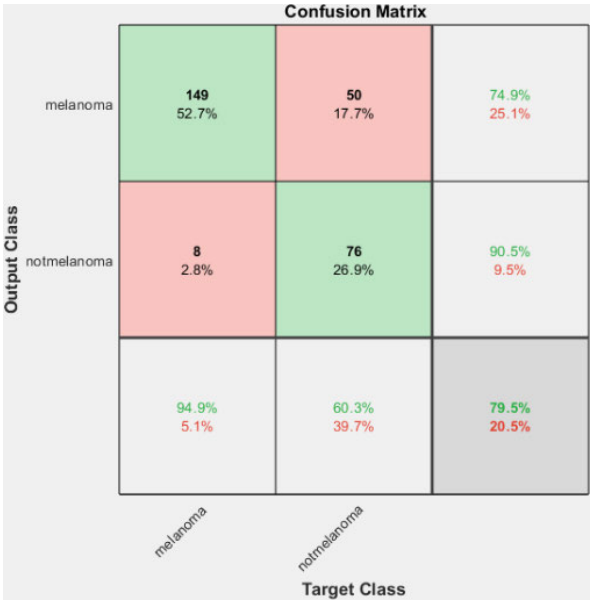

FIGURE 12. Confusion matrix of DermQuest original images with augmentation at epoch 9.

2) RESULTS FOR DermQuest DATA

Likewise, DermIS, we performed the same transfer learning approach to the second dataset namely DermQuest. All the experimentations conducted using a color image from the required database, as per the AlexNet, the image size should be 227 × 227 ×3. We checked the learning rate by varying values from le-1 up to le-10. In the same way, to reach optimum output we vary the bias and weight learn factor from le-4 to le-10 and 10-100 respectively. Figure 11 demonstrates the process of training and loss using the original DermQuest image on epoch size 9 along with the augmentation of the data approach.

We achieved 79.5% performance accuracy for original DermQuest images on epoch size 9 with augmentation. The performance rise of 1.1% is achieved as compared to results from epoch 6 with epoch 9. For skin cancer

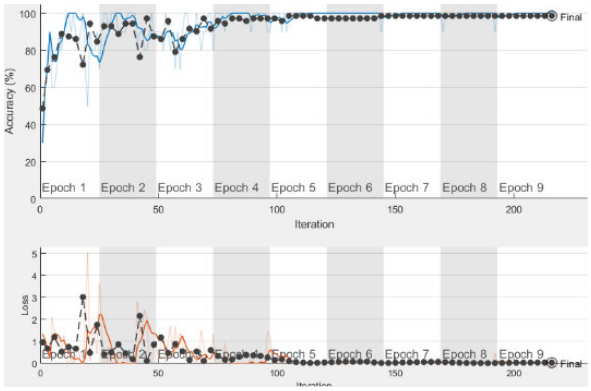

FIGURE 13. Training and loss process of ROI DermQuest with augmentation on epoch 9.

FIGURE 14. Confusion matrix of DermQuest ROI images with augmentation at epoch 9.

classification, we compared the results achieved from epochs 6, 7, and 8 with augmentation approaches and noticed that epoch 9 gives the optimum output. This AlexNet architecture acquires the training data and reached 58.30% accuracy on epoch 1, 70.67% on epoch 2, 72.24% on epoch3, 75.32% on epoch 4, 70.21% on epoch 5 and 78.41% on epoch6 and 79.15% on epoch7 for binary class skin cancer classification.

Figure 12 showing the confusion matrix of DermQuest original images with augmentation of data generated during the training at epoch 9.

We performed this transfer learning approach to the data that only contains skin cancer regions i.e. ROI instead of full images on DermQuest data samples. Figure 13 showing the process of training using the DermQuest ROI for epoch 9 with the techniques of data augmentation. We achieved 97.4% performance accuracy using the ROI images on epoch 9 with the distinct approaches of augmentation of data. There is a 6% increase in performance achieved as compared to epoch 6. For skin cancer classification, we compared the output achieved for epoch numbers 6, 7, and 8 with approaches of

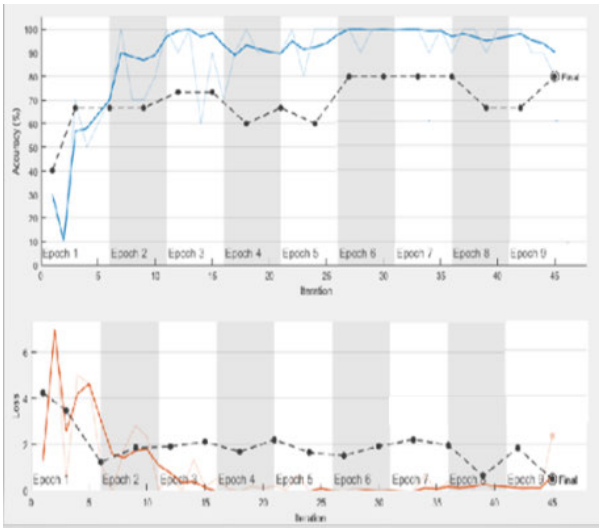

FIGURE 15. Training and loss process of DermIS ROI without the data augmentation on epoch 9.

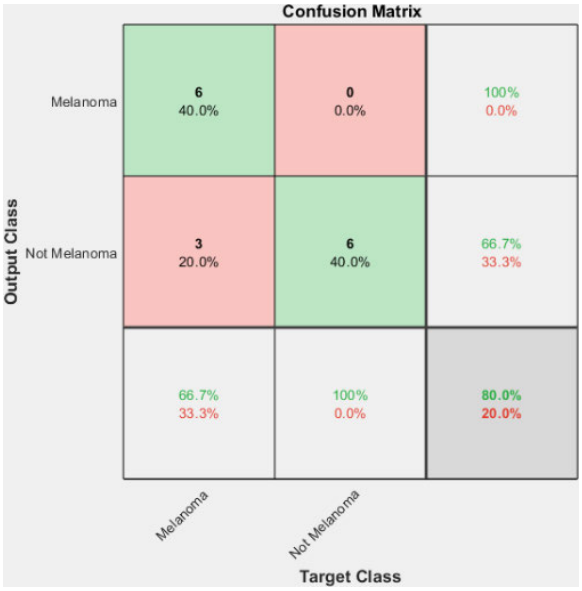

FIGURE 16. Confusion matrix of DermIS ROI without augmentation on epoch 9.

augmentation on data and come to point that epoch 9 gives the most optimum classification results. The model of AlexNet learn the data in training and achieved 81.48% performance accuracy for epoch 1, 88.89% for epoch 2, 93.65% for epoch 3, 94.18% for epoch 4, 95.77% for epoch 5 and 91.53% for epoch 6, 97.0% for epoch 7 and 95.77% for epoch 8 for binary class skin cancer classification. Figure 14 showing the confusion matrix of DermQuest ROI with augmentation of data generated during the training at epoch 9.

D. RESULTS FOR DermIS AND DermQuest WITHOUT AUGMENTATION

In this section, we have presented the results of classification without the data augmentation technique on both the dataset i.e. DermIS and DermQuest.

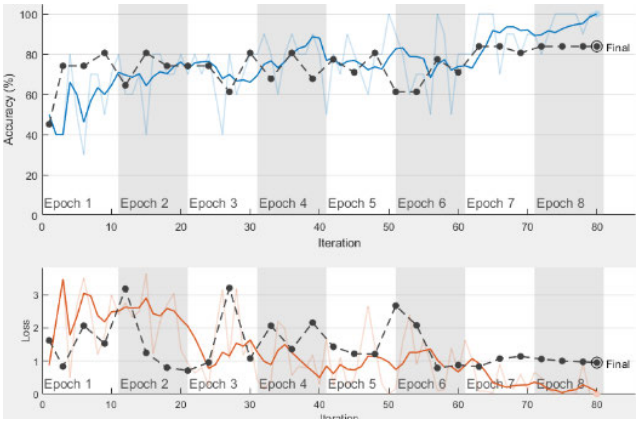

FIGURE 17. Training and loss process of DermIS original without the data augmentation on epoch 8.

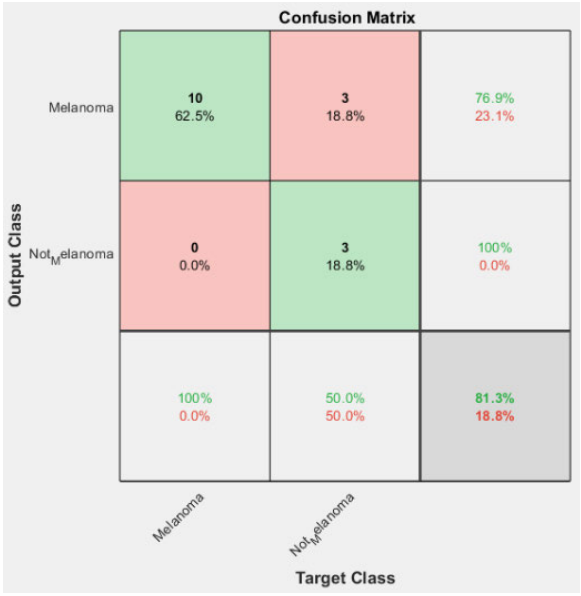

FIGURE 18. Confusion matrix of DermIS original images without augmentation at epoch 8.

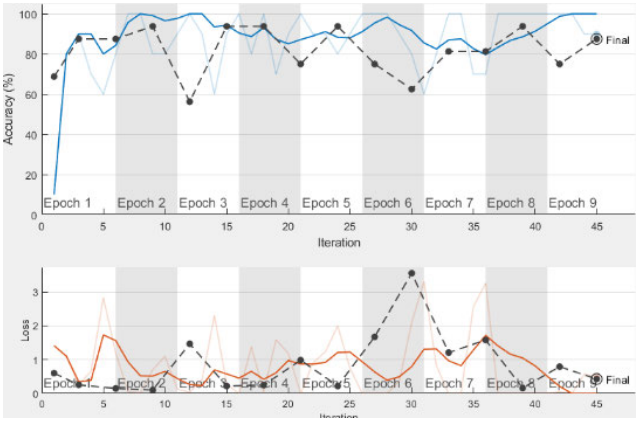

FIGURE 19. Training and loss process of ROI DermQuest without augmentation on epoch 9.

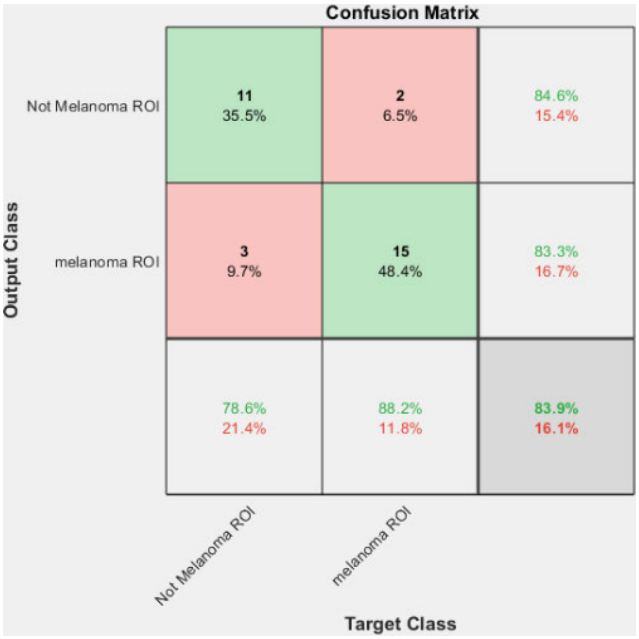

FIGURE 20. Confusion matrix of ROI DermQuest without augmentation on epoch 9.

1) RESULTS FOR DermIS

For the DermIS ROI dataset, we also used transfer learning algorithms without using the augmentation approaches on epoch sizes 6, 7, 8, and 9.

Figure 15 showing the training and loss process for the DermIS ROI on epoch 9 without using augmented data. Performance accuracy of 80.00% is achieved for the DermIS ROI without augmented data on epoch 9. Figure 16 shows the confusion matrix of ROI DermIS data without augmentation generated during the training at epoch 9.

For the DermIS original dataset, we also performed this transfer learning algorithm without the techniques of augmentation of data on epoch sizes 6, 7, 8, and 9.

Figure 17 showing the training and loss process for the original DermIS images on 8 epochs without applying augmentation techniques. In Figure 17, the blue color lines showing the performance accuracy of the training data while the black color dots showing the validation data's accuracy. We achieved the 81.30% performance accuracy for the original DermIS images without augmentation approaches on 8 epochs. Figure 18 shows the confusion matrix of DermIS original data without augmentation generated during the training at epoch 8.

2) RESULTS FOR DermQuest

For the DermQuest ROI dataset, we also used transfer learning algorithms without utilizing the approaches of data augmentation on epoch sizes 6, 7, 8, and 9. Figure 19 showing the training and loss process for the DermQuest ROI on epoch 9 without using augmented data. We achieved a performance accuracy of 83.9% for the DermIS ROI without the augmented data on epoch 9. In this Figure, the blue color lines showing the performance accuracy of the training data while the black color dots showing the validation data's accuracy. Figure 20 showing the confusion matrix of ROI DermQuest

TABLE 2. Comparison of proposed results before and after applying augmentation.

		Augmentation	Without Augmentation
DermIS	Original	97.2%	81.3%
	ROI	97.9%	80.0%
DermQuest	Original	79.5%	74.2%
	ROI	97.4%	83.9%

TABLE 3. Comparison with existing work.

Author	Dataset	Technique	Accuracy
Proposed Technique	DermIS	Transfer Learning Approach	97.2% on Original 97.9% on ROI (Augmentation)
	DermQuest		79.5% on Original 97.4% on ROI (Augmentation)
Robert et al. [9]	DermIS	SVM	94%
Robert et al.[27]	DermIS	SVM	86%
Ebthial et al.[14]	DermIS	SVM	90%
Doaa et al.[51]	DermIS	SVM	93%
M. Ali et al.[36]	DermIS	SVM	80%
Rebbeca et al.[25]	DermIS	KNN	89%
Qasim et al.[56]	DermIS	SVM	96%
Nida et al.[59]	DermIS	CNN	94.2%
Khalid et al. [58]	Derm(IS and Quest)	Transfer Learning with AlexNet	97.70%

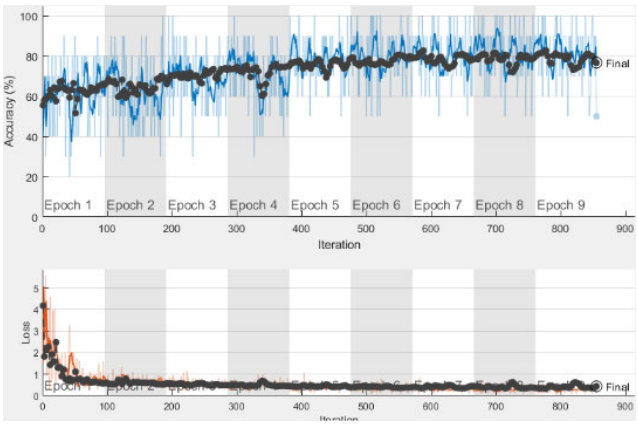

FIGURE 21. Training and loss process of original DermQuest without augmentation on epoch 9.

without the augmentation of data generated during the training at epoch 9.

For the DermQuest original dataset, we also used a transfer learning algorithm without the techniques of augmentation of data on epoch size 6, 7, 8, and 9. Figure 21 showing the training and loss process for the original DermQuest images on 9 epochs without applying augmentation techniques. We reached 74.2% performance accuracy for the original DermQuest images without augmentation approaches on 9 epochs. In Figure 21, the blue color lines showing the performance accuracy of the training data while the black color dots showing the validation data's accuracy. Figure 22 showing the confusion matrix of ROI DermQuest data without augmentation generated during the training at epoch 9.

Table 2 shows the comparison of our proposed model before and after applying augmentation approaches on both the datasets. To evaluate the performance of our system we compared our proposed model with the state-of-the-art model. Amelard *et al.* [9], Amelard *et al.* [27], Almansour and Jaffar [14], Shoieb *et al.* [51], Farooq *et al.* [36] utilizes SVM as a classifier on the DermIS database. Whereas Hosny *et al.* [58] used the transfer learning approach by using AlexNet as a pre-trained model and achieved 97.70%

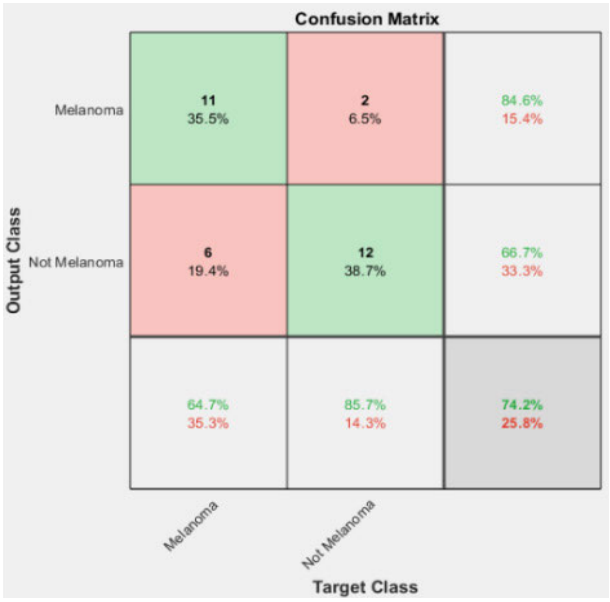

FIGURE 22. Confusion matrix of original DermQuest without augmentation on epoch 9.

accuracy. Table 3 shows the results of our proposed model with other approaches, the results show that our proposed model outperforms existing state-of-the-art approaches.

The recall and F1 for DermIS with full images are 96.8% and 96.1% while for ROI based methods are 97.5% and 97.7% respectively. The recall and F1 for DermQuest with full images are 76.9% and 76.0% while for ROI based methods are 98.1% and 97.9% respectively.

V. CONCLUSION

Skin cancer remains one of the most common and serious types of cancer. There is a strong need to design a CAD system that can extract most discriminative features automatically and can efficiently identify the patients. Researchers have used different methods to identify discriminative features for skin cancer detection. However, these methods require human expert intervention to identify these features. In this research, to correctly classify and identify skin cancer melanoma, a transfer learning-based efficient approach is proposed by using the AlexNet model. The proposed system used Region of Interest-based images that help to extract only discriminative features. Our experiments were conducted using original images as well as ROIs for both DermIS and DermQuest. In these datasets, the sample images for training have class imbalance issues. To overcome this problem, we incorporated transfer learning along with extensive augmentation approaches. We transfer the initial low-level feature layers of the AlexNet model and evaluated that ROI with augmentation gives optimum results as compared with original and without augmentation approaches.

REFERENCES

[1] M. A. Taufiq, N. Hameed, A. Anjum, and F. Hameed, "m-Skin doctor: A mobile enabled system for early melanoma skin cancer detection using support vector machine," in *eHealth 360°*. Cham, Switzerland: Springer, 2017, pp. 468–475.

[2] B. Kong, S. Sun, X. Wang, Q. Song, and S. Zhang, "Invasive cancer detection utilizing compressed convolutional neural network and transfer learning," in *Proc. Int. Conf. Med. Image Comput. Comput.-Assist. Intervent.* Cham, Switzerland: Springer, 2018, pp. 156–164.

[3] Y. Zhang, S. Wang, P. Phillips, Z. Dong, G. Ji, and J. Yang, "Detection of Alzheimer's disease and mild cognitive impairment based on structural volumetric MR images using 3D-DWT and WTA-KSVM trained by PSOTVAC," *Biomed. Signal Process. Control*, vol. 21, pp. 58–73, Aug. 2015.

[4] R. Kasmi and K. Mokrani, "Classification of malignant melanoma and benign skin lesions: Implementation of automatic ABCD rule," *IET Image Process.*, vol. 10, no. 6, pp. 448–455, Jun. 2016.

[5] R. J. Friedman, D. S. Rigel, and A. W. Kopf, "Early detection of malignant melanoma: The role of physician examination and self-examination of the skin," *CA, Cancer J. Clinicians*, vol. 35, no. 3, pp. 130–151, 1985.

[6] G. Argenziano, C. Catricalà, M. Ardigo, P. Buccini, P. De Simone, L. Eibenschutz, A. Ferrari, G. Mariani, V. Silipo, I. Sperduti, and I. Zalaudek, "Seven-point checklist of dermoscopy revisited," *Brit. J. Dermatol.*, vol. 164, no. 4, pp. 785–790, Apr. 2011.

[7] H. P. Soyer, G. Argenziano, I. Zalaudek, R. Corona, F. Sera, R. Talamini, F. Barbato, A. Baroni, L. Cicale, A. Di Stefani, P. Farro, L. Rossiello, E. Ruocco, and S. Chimenti, "Three-point checklist of dermoscopy," *Dermatology*, vol. 208, no. 1, pp. 27–31, 2004.

[8] P. Mohanaiah, P. Sathyanarayana, and L. GuruKumar, "Image texture feature extraction using GLCM approach," *Int. J. Sci. Res. Publications*, vol. 3, no. 5, p. 1, 2013.

[9] R. Amelard, J. Glaister, A. Wong, and D. A. Clausi, "High-level intuitive features (HLIFs) for intuitive skin lesion description," *IEEE Trans. Biomed. Eng.*, vol. 62, no. 3, pp. 820–831, Mar. 2015.

[10] D. O. T. Bruno, M. Z. do Nascimento, R. P. Ramos, V. R. Batista, L. A. Neves, and A. S. Martins, "LBP operators on curvelet coefficients as an algorithm to describe texture in breast cancer tissues," *Expert Syst. Appl.*, vol. 55, pp. 329–340, Aug. 2016.

[11] N. R. Abbasi, H. M. Shaw, D. S. Rigel, R. J. Friedman, W. H. McCarthy, I. Osman, A. W. Kopf, and D. Polsky, "Early diagnosis of cutaneous melanoma: Revisiting the ABCD criteria," *J. Amer. Med. Assoc.*, vol. 292, no. 22, pp. 2771–2776, Dec. 2004.

[12] R. H. Johr, "Dermoscopy: Alternative melanocytic algorithms—The ABCD rule of dermatoscopy, menzies scoring method, and 7-point checklist," *Clinics Dermatol.*, vol. 20, no. 3, pp. 240–247, May 2002.

[13] H. Kittler, M. Seltenheim, M. Dawid, H. Pehamberger, K. Wolff, and M. Binder, "Morphologic changes of pigmented skin lesions: A useful extension of the ABCD rule for dermatoscopy," *J. Amer. Acad. Dermatol.*, vol. 40, no. 4, pp. 558–562, Apr. 1999.

[14] E. Almansour and M. A. Jaffar, "Classification of dermoscopic skin cancer images using color and hybrid texture features," *Int. J. Comput. Sci. Netw. Secur.*, vol. 16, no. 4, pp. 135–139, 2016.

[15] F. Xie, H. Fan, Y. Li, Z. Jiang, R. Meng, and A. Bovik, "Melanoma classification on dermoscopy images using a neural network ensemble model," *IEEE Trans. Med. Imag.*, vol. 36, no. 3, pp. 849–858, Mar. 2017.

[16] M. B. Bonab, S. Z. M. Hashim, A. K. Z. Alsaedi, and U. R. Hashim, "Modified K-means combined with artificial bee colony algorithm and differential evolution for color image segmentation," in *Computational Intelligence in Information Systems*. Cham, Switzerland: Springer, 2015, pp. 221–231.

[17] M. Silveira, J. C. Nascimento, J. S. Marques, A. R. S. Marcal, T. Mendonca, S. Yamauchi, J. Maeda, and J. Rozeira, "Comparison of segmentation methods for melanoma diagnosis in dermoscopy images," *IEEE J. Sel. Topics Signal Process.*, vol. 3, no. 1, pp. 35–45, Feb. 2009.

[18] S. Zahra, M. A. Ghazanfar, A. Khalid, M. A. Azam, U. Naeem, and A. Prugel-Bennett, "Novel centroid selection approaches for K means-clustering based recommender systems," *Inf. Sci.*, vol. 320, pp. 156–189, Nov. 2015.

[19] F. Nachbar, "The ABCD rule of dermatoscopy: High prospective value in the diagnosis of doubtful melanocytic skin lesions," *J. Amer. Acad. Dermatol.*, vol. 30, no. 4, pp. 551–559, Apr. 1994.

[20] M. Keefe, D. C. Dick, and R. A. Wakeel, "A study of the value of the seven-point checklist in distinguishing benign pigmented lesions from melanoma," *Clin. Exp. Dermatol.*, vol. 15, no. 3, pp. 167–171, May 1990.

[21] M. F. Healsmith, J. F. Bourke, J. E. Osborne, and R. A. C. Graham-Brown, "An evaluation of the revised seven-point checklist for the early diagnosis of cutaneous malignant melanoma," *Brit. J. Dermatol.*, vol. 130, no. 1, pp. 48–50, Jan. 1994.

[22] A. Masood and A. A. Al-Jumaily, "Computer aided diagnostic support system for skin cancer: A review of techniques and algorithms," *Int. J. Biomed. Imag.*, vol. 2013, pp. 1–22, Dec. 2013.

[23] Z. Shi, H. Hao, M. Zhao, Y. Feng, L. He, Y. Wang, and K. Suzuki, "A deep CNN based transfer learning method for false positive reduction," *Multimedia Tools Appl.*, vol. 78, no. 1, pp. 1017–1033, Jan. 2019.

[24] S. Demyanov, R. Chakravorty, M. Abedini, A. Halpern, and R. Garnavi, "Classification of dermoscopy patterns using deep convolutional neural networks," in *Proc. IEEE 13th Int. Symp. Biomed. Imag. (ISBI)*, Apr. 2016, pp. 364–368.

[25] R. Moussa, F. Gerges, C. Salem, R. Akiki, O. Falou, and D. Azar, "Computer-aided detection of melanoma using geometric features," in *Proc. 3rd Middle East Conf. Biomed. Eng. (MECBME)*, Oct. 2016, pp. 125–128.

[26] G. Argenziano, H. P. Soyer, S. Chimenti, R. Talamini, R. Corona, F. Sera, M. Binder, L. Cerroni, G. De Rosa, G. Ferrara, and R. Hofmann-Wellenhof, "Dermoscopy of pigmented skin lesions: Results of a consensus meeting via the Internet," *J. Amer. Acad. Dermatol.*, vol. 48, no. 5, pp. 679–693, May 2003.

[27] R. Amelard, A. Wong, and D. A. Clausi, "Extracting high-level intuitive features (HLIF) for classifying skin lesions using standard camera images," in *Proc. 9th Conf. Comput. Robot Vis.*, 2012, pp. 396–403.

[28] M. E. Celebi, H. A. Kingravi, B. Uddin, H. Iyatomi, Y. A. Aslandogan, W. V. Stoecker, and R. H. Moss, "A methodological approach to the classification of dermoscopy images," *Comput. Med. Imag. Graph.*, vol. 31, no. 6, pp. 362–373, Sep. 2007.

[29] R. J. Stanley, W. V. Stoecker, and R. H. Moss, "A relative color approach to color discrimination for malignant melanoma detection in dermoscopy images," *Skin Res. Technol.*, vol. 13, no. 1, pp. 62–72, Feb. 2007.

[30] C. Barata, M. Ruela, M. Francisco, T. Mendonca, and J. S. Marques, "Two systems for the detection of melanomas in dermoscopy images using texture and color features," *IEEE Syst. J.*, vol. 8, no. 3, pp. 965–979, Sep. 2014.

[31] H. Ganster, P. Pinz, R. Rohrer, E. Wildling, M. Binder, and H. Kittler, "Automated melanoma recognition," *IEEE Trans. Med. Imag.*, vol. 20, no. 3, pp. 233–239, Mar. 2001.

[32] P. Rubegni, G. Cevenini, M. Burroni, R. Perotti, G. Dell'Eva, P. Sbano, C. Miracco, P. Luzi, P. Tosi, P. Barbini, and L. Andreassi, "Automated diagnosis of pigmented skin lesions," *Int. J. Cancer*, vol. 101, no. 6, pp. 576–580, Sep. 2002.

[33] R. B. Oliveira, J. P. Papa, A. S. Pereira, and J. M. R. S. Tavares, "Computational methods for pigmented skin lesion classification in images: Review and future trends," *Neural Comput. Appl.*, vol. 29, no. 3, pp. 613–636, Feb. 2018.

[34] I. Stanganelli, A. Brucale, L. Calori, R. Gori, A. Lovato, S. Magi, B. Kopf, R. Bacchilega, V. Rapisarda, A. Testori, P. A. Ascierto, P. Antonio, and E. Simeone, "Computer-aided diagnosis of melanocytic lesions," *Anticancer Res.*, vol. 25, no. 6C, pp. 4577–4582, 2005.

[35] H. Iyatomi, H. Oka, M. E. Celebi, K. Ogawa, G. Argenziano, H. P. Soyer, H. Koga, T. Saida, K. Ohara, and M. Tanaka, "Computer-based classification of dermoscopy images of melanocytic lesions on acral volar skin," *J. Investigative Dermatol.*, vol. 128, no. 8, pp. 2049–2054, Aug. 2008.

[36] M. A. Farooq, M. A. M. Azhar, and R. H. Raza, "Automatic lesion detection system (ALDS) for skin cancer classification using SVM and neural classifiers," in *Proc. IEEE 16th Int. Conf. Bioinf. Bioeng. (BIBE)*, Oct. 2016, pp. 301–308.

[37] J. F. Alcon, C. Ciuhu, W. T. Kate, A. Heinrich, N. Uzunbajakava, G. Krekels, D. Siem, and G. de Haan, "Automatic imaging system with decision support for inspection of pigmented skin lesions and melanoma diagnosis," *IEEE J. Sel. Topics Signal Process.*, vol. 3, no. 1, pp. 14–25, Feb. 2009.

[38] I. Giotis, N. Molders, S. Land, M. Biehl, M. F. Jonkman, and N. Petkov, "MED-NODE: A computer-assisted melanoma diagnosis system using non-dermoscopic images," *Expert Syst. Appl.*, vol. 42, no. 19, pp. 6578–6585, Nov. 2015.

[39] A. Safi, M. Baust, O. Pauly, V. Castaneda, T. Lasser, D. Mateus, N. Navab, R. Hein, and M. Ziai, "Computer-aided diagnosis of pigmented skin dermoscopic images," in *Proc. MICCAI Int. Workshop Med. Content-Based Retr. Clin. Decis. Support*. Berlin, Germany: Springer, 2011, pp. 105–115.

[40] M. Abedini, Q. Chen, N. C. F. Codella, R. Garnavi, X. Sun, M. E. Celebi, T. Mendonca, and J. S. Marques, "Accurate and scalable system for automatic detection of malignant melanoma," in *Dermoscopy Image Analysis*. New York, NY, USA: Taylor & Francis, Sep. 2015, Art. no. 293343.

[41] D. Ruiz, V. Berenguer, A. Soriano, and B. Sánchez, "A decision support system for the diagnosis of melanoma: A comparative approach," *Expert Syst. Appl.*, vol. 38, no. 12, pp. 15217–15223, Nov. 2011.

[42] A. Masood and A. Al-Jumaily, "Differential evolution based advised SVM for histopathalogical image analysis for skin cancer detection," in *Proc. 37th Annu. Int. Conf. IEEE Eng. Med. Biol. Soc. (EMBC)*, Aug. 2015, pp. 781–784.

[43] H. Jing, X. He, Q. Han, A. A. A. El-Latif, and X. Niu, "Saliency detection based on integrated features," *Neurocomputing*, vol. 129, pp. 114–121, Apr. 2014.

[44] M. Hammad, A. Maher, K. Wang, F. Jiang, and M. Amrani, "Detection of abnormal heart conditions based on characteristics of ECG signals," *Measurement*, vol. 125, pp. 634–644, Sep. 2018.

[45] X. Bai, T. Zhang, C. Wang, A. A. A. El-Latif, and X. Niu, "A fully automatic player detection method based on one-class SVM," *IEICE Trans. Inf. Syst.*, vol. E96.D, no. 2, pp. 387–391, 2013.

[46] M. Amrani, M. Hammad, F. Jiang, K. Wang, and A. Amrani, "Very deep feature extraction and fusion for arrhythmias detection," *Neural Comput. Appl.*, vol. 30, no. 7, pp. 2047–2057, Oct. 2018.

[47] T. Zhang, Q. Han, A. A. A. El-Lat, X. Bai, and X. Niu, "2-D cartoon character detection based on scalable-shape context and Hough voting," *Inf. Technol. J.*, vol. 12, no. 12, pp. 2342–2349, Dec. 2013.

[48] S. Wu, Z. Gao, Z. Liu, J. Luo, H. Zhang, and S. Li, "Direct reconstruction of ultrasound elastography using an end-to-end deep neural network," in *Proc. Int. Conf. Med. Image Comput. Comput.-Assist. Intervent.* Cham, Switzerland: Springer, 2018, pp. 374–382.

[49] B. Kong, Y. Zhan, M. Shin, T. Denny, and S. Zhang, "Recognizing end-diastole and end-systole frames via deep temporal regression network," in *Proc. Int. Conf. Med. Image Comput. Comput.-Assist. Intervent.* Cham, Switzerland: Springer, 2016, pp. 264–272.

[50] U.-O. Dorj, K.-K. Lee, J.-Y. Choi, and M. Lee, "The skin cancer classification using deep convolutional neural network," *Multimedia Tools Appl.*, vol. 77, no. 8, pp. 9909–9924, Apr. 2018.

[51] D. A. Shoieb, S. M. Youssef, and W. M. Aly, "Computer-aided model for skin diagnosis using deep learning," *J. Image Graph.*, vol. 4, no. 2, pp. 122–129, 2016.

[52] H. Lee and Y.-P.-P. Chen, "Image based computer aided diagnosis system for cancer detection," *Expert Syst. Appl.*, vol. 42, no. 12, pp. 5356–5365, Jul. 2015.

[53] S. Afzal, M. Javed, M. Maqsood, F. Aadil, S. Rho, and I. Mehmood, "A segmentation-less efficient Alzheimer detection approach using hybrid image features," in *Handbook of Multimedia Information Security: Techniques and Applications*. Cham, Switzerland: Springer, 2019, pp. 421–429.

[54] S. Afzal, M. Maqsood, F. Nazir, U. Khan, F. Aadil, K. M. Awan, I. Mehmood, and O.-Y. Song, "A data augmentation-based framework to handle class imbalance problem for Alzheimer's stage detection," *IEEE Access*, vol. 7, pp. 115528–115539, 2019.

[55] F. Jabeen, M. Maqsood, M. A. Ghazanfar, F. Aadil, S. Khan, M. F. Khan, and I. Mehmood, "An IoT based efficient hybrid recommender system for cardiovascular disease," *Peer-Peer Netw. Appl.*, vol. 12, no. 5, pp. 1263–1276, Sep. 2019.

[56] M. Q. Khan, A. Hussain, S. U. Rehman, U. Khan, M. Maqsood, K. Mehmood, and M. A. Khan, "Classification of melanoma and nevus in digital images for diagnosis of skin cancer," *IEEE Access*, vol. 7, pp. 90132–90144, 2019.

[57] S. Khan, A. Khan, M. Maqsood, F. Aadil, and M. A. Ghazanfar, "Optimized Gabor feature extraction for mass classification using cuckoo search for big data E-healthcare," *J. Grid Comput.*, vol. 17, no. 2, pp. 239–254, Jun. 2019.

[58] K. M. Hosny, M. A. Kassem, and M. M. Foaud, "Classification of skin lesions using transfer learning and augmentation with alex-net," *PLoS ONE*, vol. 14, no. 5, 2019, Art. no. e0217293.

[59] N. Nida, A. Irtaza, A. Javed, M. H. Yousaf, and M. T. Mahmood, "Melanoma lesion detection and segmentation using deep region based convolutional neural network and fuzzy C-means clustering," *Int. J. Med. Informat.*, vol. 124, pp. 37–48, Apr. 2019.